Received: 21 September 2022 | Revised: 11 March 2023 | Accepted: 10 April 2023

DOI: 10.1002/ca.24048

COMMUNICATION

CLINICAL ANATOMY WILEY

An anatomical study of the suboccipital cavernous sinus and its relationship with the myodural bridge complex

Xu-Hui Zhang[1] | Jin Gong[1] | Yang Song[1] | Gary D. Hack[2] | Si-Meng Jiang[3] | Sheng-Bo Yu[1] | Xue Song[1] | Jing Zhang[1] | Heng Yang[1] | Jing Cheng[1] | Hong-Jin Sui[1,4] | Nan Zheng[1]

[1]Department of Anatomy, Dalian Medical University, Dalian, China

[2]Department of Advanced Oral Sciences and Therapeutics, University of Maryland School of dentistry, Baltimore, USA

[3]Postgraduate Training Base, The 967 Hospital of the Joint Logistics Support Force, Jinzhou Medical University, Dalian, China

[4]Dalian Hoffen Preservation Technique Institution, Dalian, China

Correspondence
Nan Zheng, Department of Anatomy, College of Basic Medicine, Dalian Medical University, Dalian, China.
Email: zhengnan831016@163.com

Funding information
National Natural Science Foundation of China, Grant/Award Number: NSFC32071184; Scientific Research Fund of Liaoning Provincial Education Department, Grant/Award Number: LZ2020048

Abstract

The suboccipital cavernous sinus (SCS) and the myodural bridge complex (MDBC) are both located in the suboccipital region. The SCS is regarded as a route for venous intracranial outflow and is often encountered during surgery. The MDBC consists of the suboccipital muscles, nuchal ligament, and myodural bridge and could be a power source for cerebrospinal fluid circulation. Intracranial pressure depends on intracranial blood volume and the cerebrospinal fluid. Since the SCS and MDBC have similar anatomical locations and functions, the aim of the present study was to reveal the relationships between them and the detailed anatomical characteristics of the SCS. The study involved gross dissection, histological staining, P45 plastination, and three-dimensional visualization techniques. The SCS consists of many small venous sinuses enclosed within a thin fibrous membrane that is strengthened by a fibrous arch closing the vertebral artery groove. The venous vessels are more abundant in the lateral and medial portions of the SCS than the middle portion. The middle and medial portions of the SCS are covered by the MDBC. Type I collagen fibers arranged in parallel and originating from the MDBC terminate on the SCS either directly or indirectly via the fibrous arch. The morphological features of SCS revealed in this research could serve as an anatomical basis for upper neck surgical procedures. There are parallel arrangements of type I collagen fibers between the MDBC and the SCS. The MDBC could change the blood volume in the SCS by pulling its wall during the head movement.

KEYWORDS
Atlanto-occipital interspace, Myodural bridge complex, suboccipital cavernous sinus, upper neck surgery, venous anatomy

1 | INTRODUCTION

The unique anatomy of the suboccipital region makes it one of the most complex regions in the human body (Kontautas et al., 2005). It includes the atlanto-occipital and atlanto-axial interspaces and contains many important structures, including the suboccipital cavernous sinus (SCS) and the myodural bridge complex (MDBC). The SCS is a venous compartment that cushions the horizontal portion of the suboccipital segment of the vertebral artery (VA) and the first cervical nerve. It is located ventrally to the deep suboccipital muscles in the atlanto-occipital interspace. The SCS and the cavernous sinus are similar in: venous cushioning; the anatomical properties

of the VA and those of the petrous–cavernous internal carotid artery (vascular loops, supporting fibrous rings, transitional patterns of the arterial walls, etc.); skull base locations; embryological development; and functional and pathological features. Hence, owing to their anatomical resemblance, the venous compartment that cushions the horizontal portion of the suboccipital segment of the VA was named the SCS by Arnautović et al. (1997). The SCS is implicated in several diseases such as the meningeal arteriovenous fistulae that involve it (Crockett et al., 2019; Hiramatsu et al., 2015), the metastatic spread of cancer to the intracranial compartment (Arnautović et al., 1997), and intraoperative bleeding in the craniocervical junction area (Wang et al., 2016).

The SCS communicates with the suboccipital venous plexus (SVP) (Arnautović et al., 1997) and the superior jugular bulb (Arnautović et al., 1997; Takahashi et al., 2005) in the suboccipital region. It also communicates with intracranial venous sinuses such as the sigmoid sinus, anterior condylar confluence (JIANG et al., 2022; Tanoue et al., 2010), and occipital sinus (Arnautović et al., 1997). Also, the two sides of the SCS communicate with each other via the internal vertebral venous plexus (VVP) (Arnautović et al., 1997). Hence, the SCS is regarded as a functional component of the vertebral venous system and acts as a "relay station" for intracranial venous drainage (Arnautović et al., 1997). Although the SCS and its communicating veins can easily be identified on MR images or multidetector row CT (Takahashi et al., 2005; Tanoue et al., 2010), its communicating veins and shape are complex and exhibit numerous variations (Chen et al., 2004; JIANG et al., 2022). Precise anatomical characterization is urgently needed.

The myodural bridge (MDB) is a fibrous connection between the suboccipital muscles and the cervical spinal dura mater (SDM) (Hack et al., 1995) and is mainly composed of type I collagen fibers (Zheng et al., 2018). It originates from the rectus capitis posterior minor (RCPmi), rectus capitis posterior major (RCPma), and obliqus capitis inferior (OCI) muscles, and the nuchal ligament (Hack et al., 1995; Pontell et al., 2013; Scali et al., 2013; Zheng et al., 2014). Further studies revealed that MDB fibers with different origins are linked to each other, and some of them fuse together. Contraction of these muscles generates a force that travels to the SDM through the MDB fibers during head movement. Actually, the fibrous connective tissue, muscles, and ligaments work together and form a structural and functional unit named the "MDBC"(Zheng et al., 2020), which effectively pulls the SDM and changes the negative pressure in the subarachnoid space. Thus, the MDBC could affect cerebrospinal fluid (CSF) circulation (Yuan et al., 2016; Zheng et al., 2020).

The SCS and the MDBC have similar anatomical locations in the atlanto-occipital interspace. The SCS is a major route for venous intracranial outflow, and the MDBC could be considered a significant power source for CSF circulation. Both structures are involved in regulating intracranial pressure. The aim of the present study is therefore to reveal the anatomical relationships between them, and the structural characteristics of the SCS.

2 | MATERIALS AND METHODS

A total of 18 formalin-fixed head and neck specimens of males aged about 50–80 years were used in this research. Specimens showing abnormal anatomical variations, trauma, inflammation, or mass lesions in the suboccipital region were excluded. The 18 specimens were divided into three groups: gross anatomy group (six specimens), histological study group (six specimens), and P45 sheet plastination group (six specimens).

The authors state that every effort was made to follow all local and international ethical guidelines and laws that pertain to the use of human cadaveric donors in anatomical research (Iwanaga et al., 2022). The present study was approved by the Ethics Committee of the Center for Human and Organ Donation at Dalian Medical University.

2.1 | Gross anatomy of the suboccipital region

Six specimens were used for gross dissection. Xylene and silica gel were combined, and a curing agent and oil paint (red or blue) were added to prepare red and blue perfusates, which were used to perfuse the internal carotid and vertebral arteries (red), and the internal jugular veins (blue). After the perfusions were completed, the specimens were left undisturbed for 48 h for the perfusates to harden within the vessels. The specimens were then fixed in formalin for 1 week.

A longitudinal incision was made from the external occipital protuberance to the spinous process of the seventh cervical vertebra. A transverse incision was then made along the inferior nuchal line to the mastoid processes. Another transverse incision was made along the spinous process of the seventh cervical vertebra. The suboccipital region was then dissected from superficial to deep until the suboccipital triangle was exposed. The obliquus capitis superior (OCS) muscle was detached from its occipital attachment and directed to the inferolateral side. The OCI muscle was separated from its attachment on the transverse process of the atlas and directed to the inferomedial side. The RCPma muscle was separated from its occipital attachment and reflected medially. The RCPmi muscle was reflected from its occipital attachment to the inferior side. The location of SCS and its communicating veins, and the connection between the SCS and the MDBC, were noted.

2.2 | Histological study

Six specimens were used for histological examination. First, the OCS and OCI muscles were cut off along their origins. The RCPma muscles were reflected at their occipital attachments to expose the occiput. A reciprocating saw was used to separate the occiput from the rest. Also, the attachments of the RCPma muscles on the axis were reflected. An incision was made along the posterior interspace between the atlas and the axis, and two longitudinal incisions were made along the transverse foramen of the atlas to the mastoid

processes on both sides to separate the tissue from the rest of the vertebrae. The tissue blocks, about 4.8 x 2.3 x 3.2 cm^3, which included the RCPma and RCPmi muscles, the SCS, some bone near the foramen magnum, the atlas, and the SDM, were separated from the specimens and placed in phosphate buffered saline for 2 h to remove any remaining formalin. They were then incubated in ethylene diamine tetraacetic acid (EDTA) solution for 5 months at 37°C to decalcify them. Finally, they were soaked in a sodium sulphate solution for 24 h and then rinsed under running water for 24 h. Standard dehydration, transparency, and paraffin embedding procedures were applied. The embedded tissue blocks were cut into slices about 13–20 mm thick.

These slices were divided into three groups, which were stained with hematoxylin and eosin (HE), Masson trichrome (Masson), and picric acid-sirius red, respectively. The histological characteristics of the SCS and its anatomical relationships with the MDBC were recorded.

2.3 | P45 sheet plastination of the head and neck

Six specimens were sliced sagittally in preparation for P45 sheet plastination. The morphological relationships between the SCS and the MDBC were recorded from the P45 plastinated specimens. The experimental procedure was as follows (Gao et al., 2006; Sui & Henry, 2007):

Slicing. The formalin-fixed head and neck specimens were frozen at −70°C for 2 weeks, embedded in polyurethane foam, and then frozen again at −70°C for 2 days. After freezing and smoothing the tissue blocks, 3-mm sagittal slices were made from side to side using a high-speed band saw.

Bleaching. All the slices were rinsed under cold running water overnight and then immersed again overnight in 5% dioxygen.

Dehydration. After bleaching, the slices were dehydrated using 100% acetone at −25°C, −15°C, and finally room temperature using the freeze substitution method.

Casting and forced impregnation. After dehydration, the casting molds were made. The slices were removed from the acetone bath and placed between two tempered glass plates. The molds were then filled with polyester (Hoffen polyester P45, Dalian Hoffen Bio-Technique Co. Ltd., Dalian, P. R. China). The absolute pressure was slowly decreased from 20 mm Hg to 10 mm Hg, 5 mm Hg, and finally 0 mm Hg in accordance with the observed release of bubbles. The pressure was kept at 0 mm Hg until bubbling completely stopped. The time for impregnation was at least 8 h.

Curing. After the vacuum had been released, we checked for and removed any air bubbles remaining within the sheets. The top of the mold was clamped with a large fold-back clamp, and then the sheets were placed upright in a water bath at 40°C for 3 days.

Cutting and sanding the molds. After curing, the sheets were removed from the water bath and cooled to room temperature. The sections were then protected by covering them with an adhesive plastic wrap. A band saw was used to cut and trim the plastic along the edges about 1 mm outside the slices, and the sharp edges of the slices were smoothed using a wood sander. The adhesive plastic wrap was then removed.

3 | THREE-DIMENSIONAL VISUALIZATION MODELS OF THE SCS

3.1 | Image acquisition

A total of 66 images were obtained from the Korean Digital Human Database (Park et al., 2009). Sections from a middle-aged man with the horizontal portion of the VA and its surrounding veins were selected.

3.2 | Image segmentation

The structures of interest (SOI) were the SCS, VA, RCPma muscles, RCPmi muscles, MDB, SDM, occipital bone, atlas, axis, and spinal cord. According to their anatomical locations, colors, and textures, these structures were segmented using Photoshop software. Each structure was taken as a single layer and filled with a different RGB color.

3.3 | Calculating three-dimensional (3D) models

The 3D model images were imported into the Mimics Innovation Suite 18.0 software package. We set the pixel size and layer thickness in the Scan Resolution software tabs to $x = 0.1$ mm, $y = 0.1$ mm, $z = 0.2$ mm, and we set the picture orientation. Threshold segmentation was used to segment the structures, and the growing region was used to display the structure independently. Finally, the 3D model was calculated to elucidate the morphology and structural relationships of the SOI.

The relationships between the SCS and the MDBC (RCPmi and RCPma muscles), and the morphological characteristics of the SCS, were observed and recorded.

4 | RESULTS

4.1 | The morphological characteristics of the SCS and its communications

The 3D morphology and anatomical location of the SCS were clearly shown in the 3D visualization model: the SCS lies in the atlanto-occipital interspace (Figure 1A). Its origin is located in the transverse foramen of the atlas and its termination in the dural penetration of the VA (Figure 1B). It cushions the horizontal portion of the suboccipital segment of the VA and the first cervical nerve (Figure 2B). Its shape is irregular. The SCS consists of many small venous sinuses (Figure 2B), which are enclosed by a thin fibrous membrane

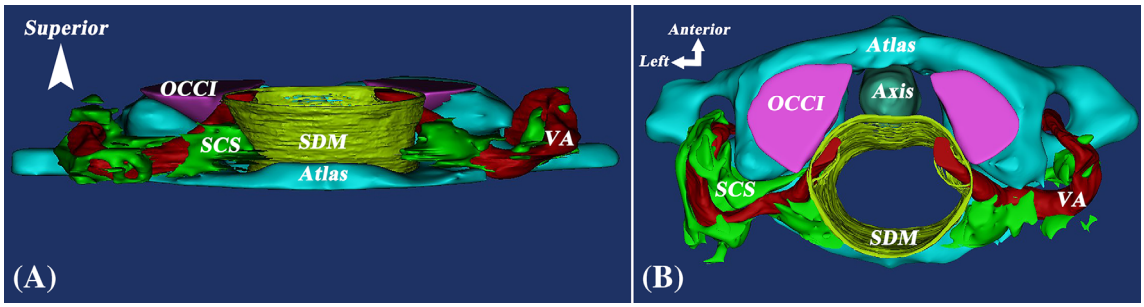

FIGURE 1 Anatomical location characteristics of the SCS shown via three-dimensional visualization models. Pictures (A) and (B) are the three-dimensional visualization models of the SCS. A (dorsal view) shows that the SCS is located in the atlanto-occipital interspace. B (upper view) shows the SCS extending from the transverse foramen of the atlas to the VA-dural junction. SCS = suboccipital cavernous sinus; VA = vertebral artery; OCCI = occipital bone; SDM = spinal dura mater.

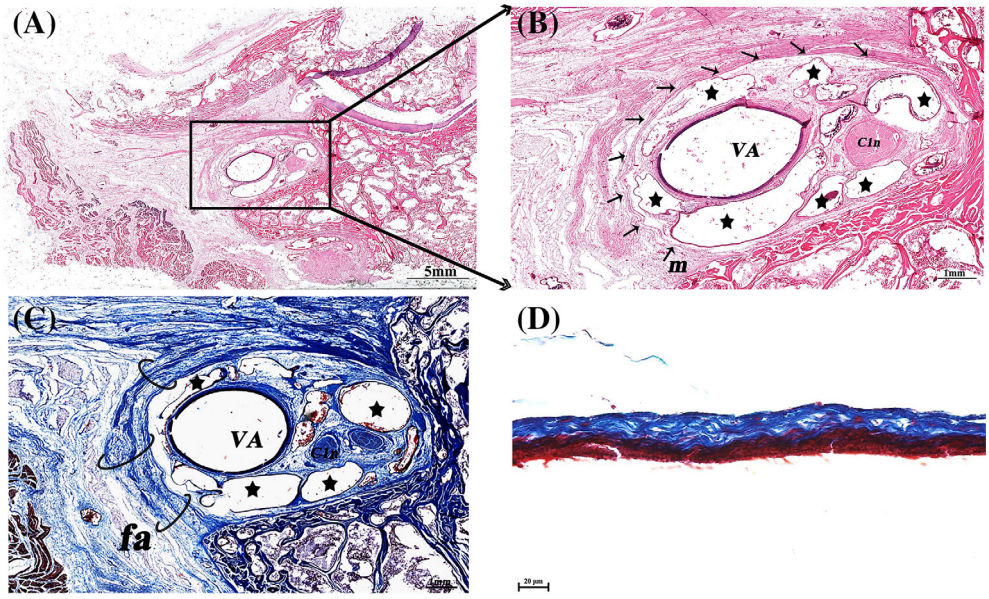

FIGURE 2 Morphological characteristics of the SCS shown via histological slices. Pictures (A) and (B) (hematoxylin–eosin-stained sections of the SCS) show that the SCS cushions the horizontal portion of the suboccipital segment of the VA and consists of many small venous sinuses enclosed by a thin fibrous membrane. Picture (C) shows that this membrane is fused with and strengthened by a fibrous arch, which closes the vertebral artery groove. Picture (D) (Masson's trichrome-stained sections of the SCS) shows that the membrane of these small venous sinuses in the SCS is very thin and consists mainly of collagen fibers. VA = vertebral artery; m (arrow) = membrane of suboccipital cavernous sinus; fa(arc) = fibrous arch; C1n = first cervical nerve; Star: suboccipital cavernous sinus.

(Figure 2B) that forms the wall of the SCS (Figure 2B). This wall is fused with and strengthened by a fibrous arch, which closes the vertebral artery groove (Figure 2C). The membrane enclosing the small venous sinuses is very thin and consists mainly of collagen fibers (Figure 2D).

The SCS can be divided into three portions, reflecting its relationship with adjacent anatomical structures. The lateral portion extends between the transverse foramen of the atlas and the vertebral artery groove. The middle portion is located in the vertebral artery groove. The medial portion extends between the vertebral artery groove and the dural entry point of the VA (Figure 3A, B). The lateral portion is mostly located dorsally to the posterior atlanto-occipital membrane (PAOM). The middle portion is mainly located within the PAOM and the medial portion ventrally to it (Figure 4C). The abundance of venous sinuses inside the SCS differs among its three parts: the lateral and medial portions have more venous sinuses than the middle (Figure 5A, B, and C). However, the venous sinuses in the lateral and the medial portions become more sparse when the SCS passes through the transverse foramen of the atlas, and continues with the dura mater, respectively (Figure 5D, E).

Two anastomotic veins pass through the suboccipital triangle to communicate with the SVP and the VVP (Figure 6A, C), and they communicate with the SCS beneath the suboccipital muscles (Figure 6B, C).

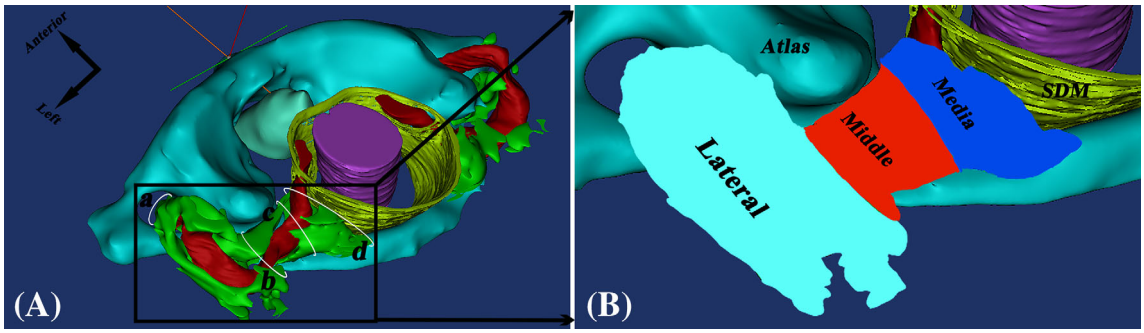

FIGURE 3 Anatomical division of the SCS shown via three-dimensional visualization models. Pictures (A) and (B) show the SCS can be divided into three portions. The lateral portion (from a to b) extends between the transverse foramen of the atlas and the vertebral artery groove. The middle portion (from b to c) is located in the vertebral artery groove. The medial portion (from c to d) extends between the vertebral artery groove and the dural entry point of the VA. SDM = spinal dura mater

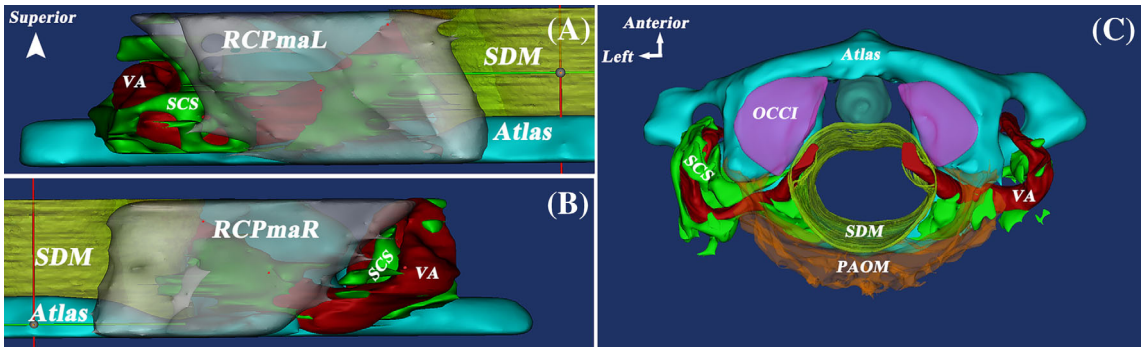

FIGURE 4 The relationship between the SCS and surrounding structures shown via three-dimensional visualization models. Pictures (A) and (B) show that the middle and medial portions of the SCS are covered by the RCPma muscle. Picture (C) shows the lateral portion of SCS, which is mostly located dorsally to the PAOM. The middle portion is mainly located within the PAOM and the medial portion is primarily located ventrally to it. RCPmaL = left rectus capitis posterior major muscle; RCPmaR = right rectus capitis posterior major muscle; VA = vertebral artery; SCS = suboccipital cavernous sinus; SDM = spinal dura mater; PAOM = posterior atlantooccipital membrane; OCCI = occipital bone.

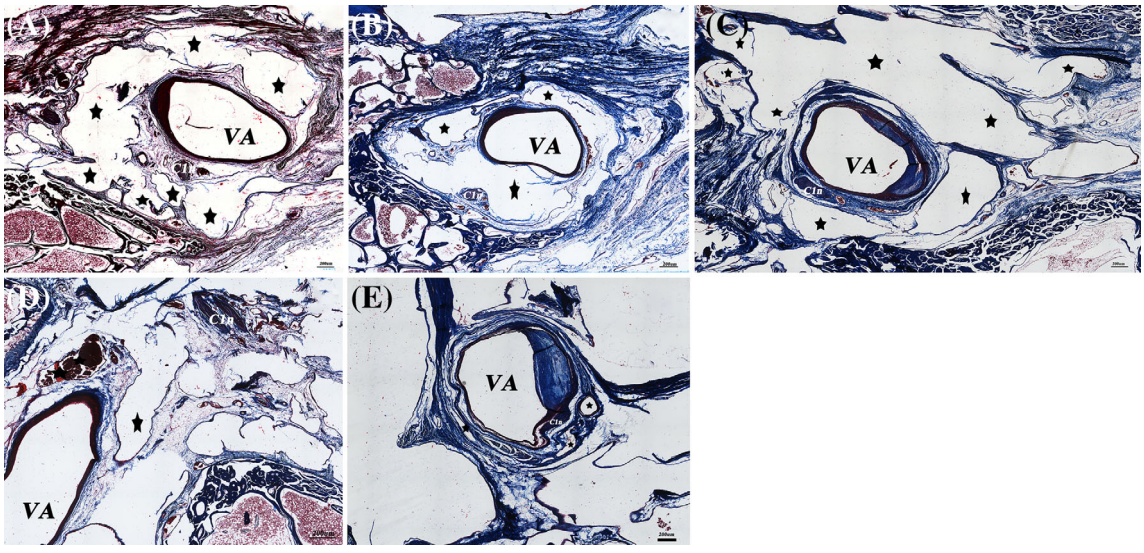

FIGURE 5 The richness of venous sinuses within SCS shown via histological slices. All the pictures are from parasagittal sections with Masson's trichrome staining. Pictures (A), (B), and (C) show the lateral, middle, and medial portions of the SCS, respectively. Picture (D) shows the SCS to be located at the transverse foramen of the atlas. Picture (E) shows it located where the VA crosses the dura. The abundance of venous sinuses inside the SCS differs among its three portions; they are more abundant in the lateral and medial portions than the middle. The venous sinuses in the lateral and medial portions become fewer when the SCS passes through the transverse foramen of the atlas, and continues with the dura mater, respectively. VA = vertebral artery; Star: suboccipital cavernous sinus; C1n = first cervical nerve.

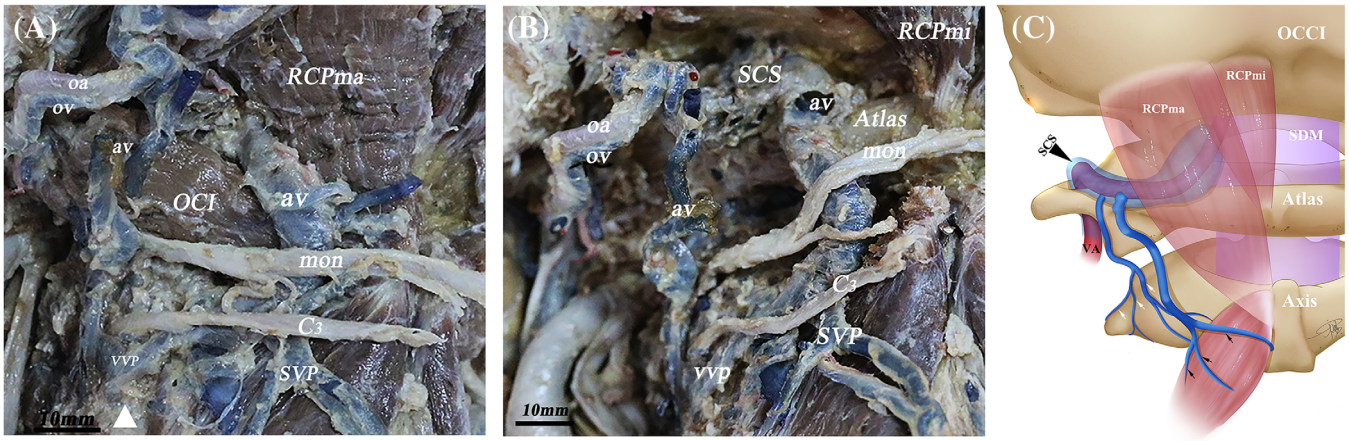

FIGURE 6 Gross anatomy of the human suboccipital region showing the veins that communicate with the SCS. Picture (A) shows the two anastomotic veins that pass through the suboccipital triangle to communicate with the SVP and the VVP. Picture (B) shows the anastomotic veins communicating with the SCS after the suboccipital muscles have been removed. Picture (C), a schematic drawing, shows that the middle and medial portions of the SCS are covered by the RCPma muscle, and the SCS communicates with the SVP and the VVP. White triangle: third cervical vertebra; RCPma = rectus capitis posterior major muscle; RCPmi = rectus capitis posterior minor muscle; OCI = obliquus capitis inferior muscle; SCS = suboccipital cavernous sinus; oa = occipital artery; ov = occipital vein; vvp = vertebral venous plexus; svp = suboccipital venous plexus; VA = vertebral artery; av = anastomotic vein; mon = major occipital nerve; C3 = dorsal branch of the third cervical nerve.

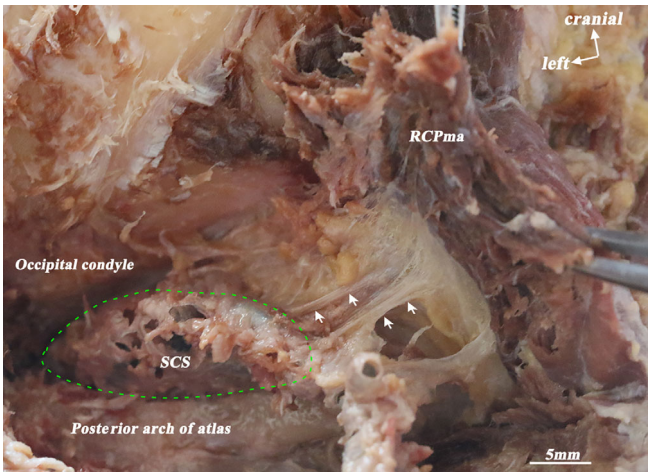

FIGURE 7 Gross anatomy of the human suboccipital region showing the fibrous connections between the RCPma muscle and the SCS. The figure shows the connections (white arrowheads) arising from the ventral surface of the RCPma muscle that terminate on the SCS. RCPma = rectus capitis posterior major muscle; SCS = suboccipital cavernous sinus.

4.2 | The anatomical relationships between the MDBC and the SCS

The relationships between the SCS and MDBC were clear in the 3D visualization model. The MDBC (RCPma muscles) covers the middle and medial portions of the SCS in the atlanto-occipital interspace (Figure 4A, B). The connective tissue fibers arising from its ventral surface (RCPma muscles) terminate at the SCS (Figure 7). These fibers are aligned in parallel and run anteroinferiorly. They connect with the wall of the SCS in two distinct ways. Some of them pass through the middle part of the atlanto-occipital interspace and terminate at the fibrous arch that encloses the vertebral artery groove and is fused with the wall of the SCS. Hence, fibers originating from the MDBC connect indirectly with the wall of the SCS via the fibrous arch (Figures 8A, 10A). Others pass through the inferior portion of the PAOM and connect with the wall of the SCS directly (Figures 8B, 10B).

Masson's trichrome staining revealed that some of these fibers are MDB fibers (Figure 9B). Other fibers pass through the superior portion of the PAOM, connecting directly with the wall of the SCS (Figures 9A, 10B).

In the picric acid-sirius-stained sections the fibrous connection between the SCS and the MDBC was stained dark red, indicating that these fibers are collagen (Figure 11A). Under polarizing microscopy they were red or yellow, showing that the collagen is mainly Type I (Figures 11B, C). These type I collagen fibers show strong double refraction.

5 | DISCUSSION

5.1 | Clinical significance of the morphological characteristics of the SCS

A venous compartment in the atlanto-occipital interspace cushions the horizontal portion of the suboccipital segment of the VA and the first cervical nerve. It was named the "SCS" by Arnautović et al. (1997). Its appearance varies greatly in MRI images; it can be oval or irregular (Chen et al., 2004). However, statistical analysis revealed no significant gender differences in the volume of SCS or its distance from the midline on the left and right sides (Chen et al., 2011). The

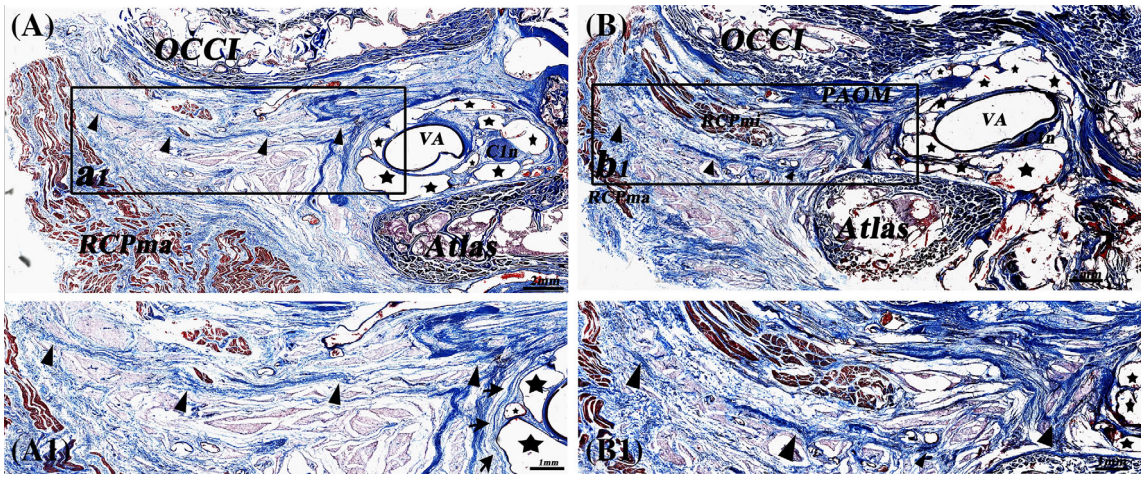

FIGURE 8 The fibrous connections between the SCS and the MDBC (RCPma muscles) revealed in Masson's trichrome stained sections (parasagittal sections). Picture (A) shows fibers originating from the ventral surface of the RCPma muscle arranged in parallel and running anteroinferiorly. These fibers pass through the atlanto-occipital interspace and terminate at the fibrous arch enclosing the vertebral artery groove. The fibrous arch is fused with the wall of the SCS. Picture (B) shows fibers originating from the ventral surface of the RCPma muscle arranged in parallel and running anteroinferiorly. These fibers pass through the inferior portion of the PAOM and connect directly with the wall of the SCS. RCPma = rectus capitis posterior major muscle; RCPmi = rectus capitis posterior minor muscle; C1n = first cervical nerve; VA = vertebral artery; PAOM = posterior atlantooccipital membrane. A1 = Enlargement of figure a1; B1 = Enlargement of figure b1; OCCI = occipital bone; Star: suboccipital cavernous sinus; arrowhead: fibrous arch; triangle: fibrous connection.

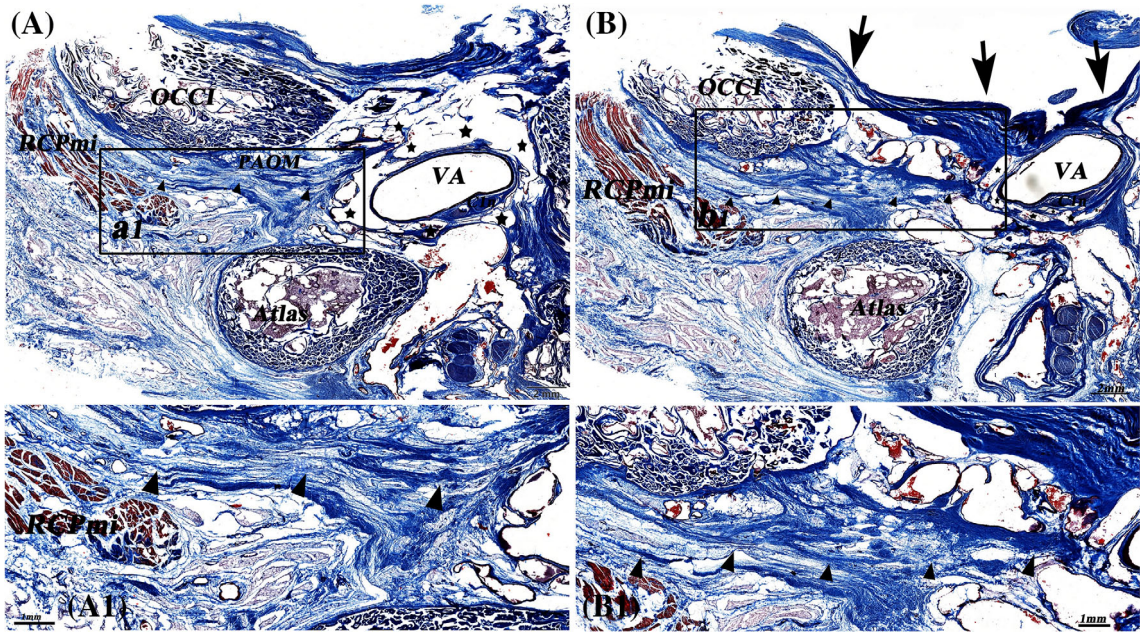

FIGURE 9 The fibrous connection between the SCS and the MDBC (RCPmi muscles) revealed in Masson's trichrome stained sections (parasagittal sections). Picture (A) shows the fibers originating from the ventral surface of the RCPmi muscle running anteroinferiorly, passing through the PAOM, and terminating directly on the SCS. Picture (B) shows the MDB fibers originating from the ventral surface of the RCPmi muscle, running anteroinferiorly, passing through the PAOM, and connecting directly to the SCS. RCPmi = rectus capitis posterior minor muscle; C1n = first cervical nerve; VA = vertebral artery; PAOM = posterior atlantooccipital membrane; OCCI = occipital bone; A1 = Enlargement of figure a1; B1 = Enlargement of figure b1; Arrowhead = dura mater; Star: suboccipital cavernous sinus; triangle: fibrous connection.

abundance of venous sinuses inside the SCS differed among its three portions; they were less abundant in the middle than the other two portions.

In clinical surgery, Ibn Essayed and Al-Mefty (2021) mentioned that the SCS could be encountered in the transcondylar decompression approach for craniovertebral junction lesions. Wang et al. (2016)

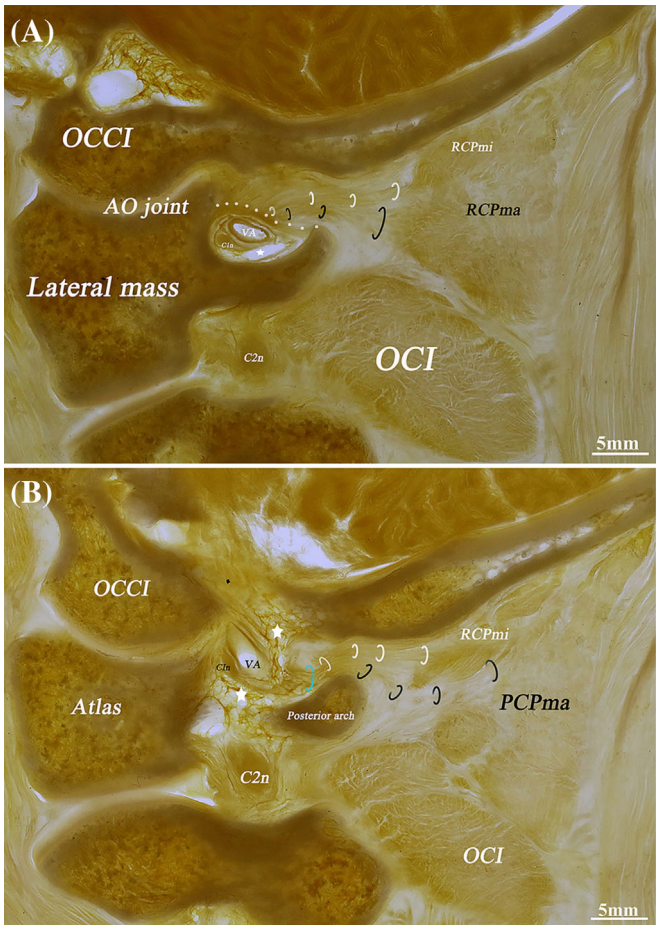

FIGURE 10 The fibrous connections between the SCS and the MDBC (RCPma muscles and RCPmi muscles) revealed by P45 plastinated sheets (parasagittal sections). Picture (A) shows the fibers originating from the ventral surfaces of the RCPma and RCPmi muscles, which are arranged in parallel and run anteroinferiorly to connect with the fibrous arch covering the SCS. Picture (B) shows that the ventral surfaces of the RCPma and RCPmi muscles give off connective fibers that pass through the lower and upper aspects of the PAOM, respectively, and then fuse together to terminate directly on the SCS. Dot: fibrous arch; arc: fibrous connection; start: suboccipital cavernous sinus. RCPma = rectus capitis posterior major muscle; RCPmi = rectus capitis posterior minor muscle; OCI = obliquus capitis inferior muscle; C1n = first cervical nerve; C2n = dorsal branch of the second cervical nerve; VA = vertebral artery; OCCI = occipital bone; AO joint = atlanto-occipital joint. PAOM = posterior atlantooccipital membrane.

reported that the SCS, the vertebral artery venous plexus, and the VVP are the main sources of hemorrhage during surgery for tumors involving the upper cervical peripheral nerve sheath. Haffajee et al. (2008) also proposed that injury to the extensive venous plexus (such as cavernous-like veins) around the craniocervical junction should be avoided because it can cause hemorrhage. Jagetia et al. (2019) suggested that the venous channels on the posterior arch of the atlas, i.e., the SCS, are tortuous and can be injured when the dura is handled. These studies indicate that the SCS is easily encountered, and bleeding from it should be an important consideration for the surgeon. The present study shows that it can also be easily encountered in gross anatomy investigations, and the membrane surrounding the small venous sinuses within it is very thin and mainly composed of collagen fibers; so the SCS is easy to injure, leading to bleeding.

Efforts to avoid injuring the SCS during operations are worthwhile. Abidin et al. (Geyik et al., 2021; Hanakita et al., 2019) suggested that subperiosteal dissection of the SCS (paravertebral plexus surrounding the VA) is crucial for obtaining a clear operative field in diseases of the craniovertebral junction. Some authors have proposed that preservation of the fibrous membrane or wall surrounding the SCS will minimize bleeding (Wang et al., 2016). The thin fibrous membrane surrounding numerous venous sinuses identified in this research is the wall of SCS. The middle portion of the SCS, located at the vertebral artery groove, is covered by a thick fibrous arch. This strengthens the SCS wall and protects the vascular structure.

Our research findings suggest that careful surgical management can reduce the risk of injury to the SCS and reduce intraoperative bleeding. That is, the SCS in the vertebral artery groove is given priority when subperiosteal dissection of the SCS is performed during the lateral suboccipital approach. The first reason is that the wall of SCS is protected by a thick fibrous arch in this area. The second is that the venous sinuses are less abundant in the middle portion than in the other two portions.

5.2 | Physiological significance of the relationships between the SCS and the MDBC

A previous study reported CSF flow waveform parameters at the craniocervical junction before and after head rotation, obtained through cine phase-contrast MR imaging. The maximum and average CSF flow rates (0.81 ± 0.34 to 0.98 ± 0.36 mL/s, and 0.43 ± 0.20 to 0.56 ± 0.24 mL/s, respectively) increased significantly after the head rotations (Xu et al., 2016). When the OCI muscles of beagles were electrically stimulated, the CSF pressure increased significantly from 12.41 ± 4.58 to 13.45 ± 5.16 mmHg (Ma et al., 2021). Also, application of electrical stimulation to the suboccipital muscles of an American alligator increased the CSF flow velocity and reduced the CSF pressure significantly (Young et al., 2020). These studies suggest that contraction of the suboccipital muscles is important in CSF flow. The MDB fibers were regarded as a fibrous connection between the suboccipital muscles and the SDM. These muscles and fibers work together to form a structural and functional unit, the MDBC (Zheng et al., 2020). It was believed that by pulling on the SDM, the MDBC could change the negative pressure of the subarachnoid space and affect CSF flow (Yuan et al., 2016; Zheng et al., 2020), so it could be involved in the mechanism of CSF dynamics. The MDBC also participates in maintaining the integrity of the subarachnoid space and cerebellomedullary cistern to ensure smooth CSF flow and could be involved in a dural tension monitoring system to prevent in-folding of the dura mater during head movement (Enix et al., 2014; Pontell et al., 2013; Scali et al., 2013; Venne et al., 2017). In addition, pathological changes in the MDBC are involved in chronic headaches and cervical

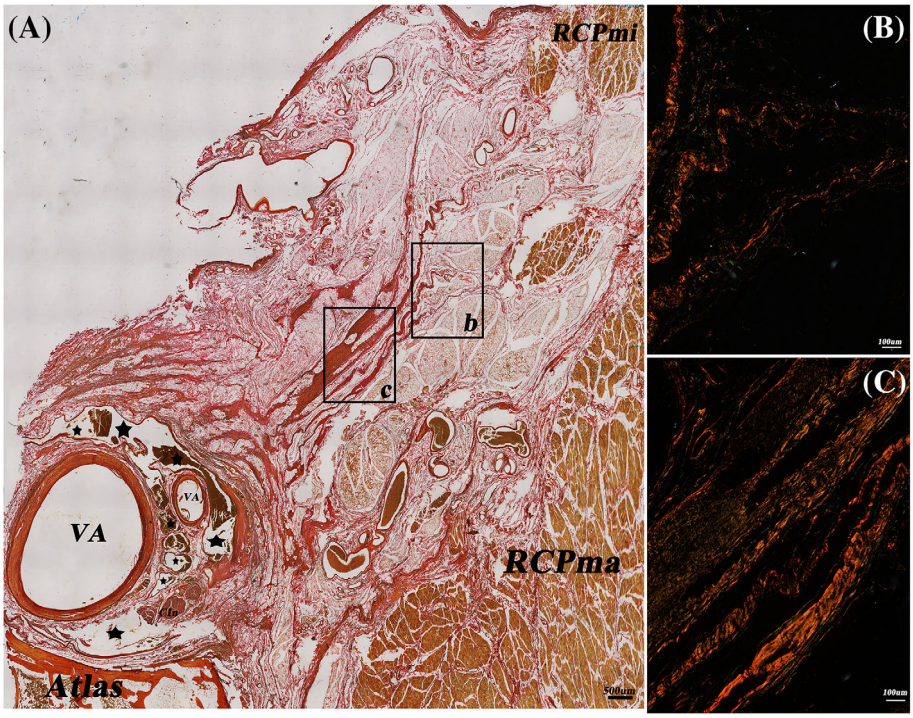

FIGURE 11 The fibrous connection between the SCS and the MDBC (RCPmi muscles and RCPma muscles) revealed by picric acid-sirius red-stained sections (parasagittal sections). Picture (A) shows the fibrous connection between the SCS and the MDBC, which was stained dark red, indicating that these fibers are collagen. Figures (B) and (C) show that they stained red or yellow, which indicates that the collagen is mainly type I. These fibers show strong double refraction. RCPma = rectus capitis posterior major muscle; RCPmi = rectus capitis posterior minor muscle; C1n = first cervical nerve; VA = vertebral artery; Star: suboccipital cavernous sinus; B = Enlargement of figure b; C = Enlargement of figure c.

proprioception transmission (George & Tadi, 2022; Hack & Hallgren, 2004; Kitamura et al., 2019; Pontell et al., 2013; Scali et al., 2013; Yuan et al., 2016; Yuan et al., 2017). Our morphological results revealed a fibrous connective tissue bridge between the wall of the SCS and the MDBC, i.e., the RCPma and RCPmi. These connections are arranged in close-packed parallel fibers mainly composed of type I collagen, so they are tuned to mechanical requirements and can transmit forces generated by muscles (Holmes et al., 2018; Testa et al., 2017). Furthermore, some of these fibers are MDB fibers, so they could transmit force from the MDBC to the SCS while the head is moving. The fibers of the SCS wall are continuous with the membrane fibers of the venous sinus inside the SCS, so traction on the SCS wall would affect not only that wall but also the wall of the venous sinus. It is therefore speculated that the MDBC could change blood circulation within the SCS via these fibrous connective tissue bridges during the contraction or relaxation of these muscles. In addition, because the SCS communicates with the VVP, it has been regarded as a functional component of the vertebral venous system, a major route for cerebral venous outflow (Arnautović et al., 1997; Carpenter et al., 2021). This communication was also observed in our research, and several communicating vessels were found between the SCS and intracranial venous sinuses and the internal jugular vein. Some researchers have considered the SCS to function as a more independent and important relay station in cerebral venous outflow (Arnautović et al., 1997; JIANG et al., 2022; Takahashi et al., 2005). We therefore speculated that this potential change in blood circulation in the SCS alters the intracranial blood circulation. Also, intracranial pressure results from interactions between the brain, CSF, and cerebral blood volume, and the VVP is important in regulating it (Nathoo et al., 2011; Nowaczewska & Kaźmierczak, 2019). Interestingly, Arnautović et al. (1997) suggested that the horizontal portion of the suboccipital segment of the VA is cushioned by the SCS and that the intraluminal pressures and pulsations in the former are interrelated with the pressures in the latter. This apparently affects intracranial pressure in some manner. Our results suggest a possible explanation for the mechanism by which the SCS regulates intracranial pressure.

However, the limitation of this study is that only morphological results were obtained. Our next study will describe functional experiments to test this speculation about the role of SCS in regulating intracranial pressure.

6 | CONCLUSIONS

The richness of veins contained in the SCS varies according to its location. The middle portion is strengthened by a fibrous arch that closes the vertebral artery groove. The detailed morphological characteristics of the SCS can serve as an anatomical basis for surgical procedures in the craniocervical junction area. Parallel type I collagen fibers are arranged between the MDBC and the SCS. The MDBC could change the blood volume of the SCS by pulling its wall during head movement.

ACKNOWLEDGMENTS

The authors sincerely thank those who donated their bodies to science so that anatomical research could be performed. Results from such research can potentially increase mankind's overall knowledge, which can then improve patient care. Therefore, these donors and their families deserve our highest gratitude (Joe et al., 2021). The

authors also thank Min Suk Chung and Beom Sun Chung for providing the Visible Korean project digital image database, and are very grateful to Muhammad Adeel Alam Shah at Dalian Medical University for helping with language editing.

ORCID

Xu-Hui Zhang https://orcid.org/0000-0002-5209-2344
Nan Zheng https://orcid.org/0000-0002-5969-5420

REFERENCES

Arnautović, K. I., et al. (1997). The suboccipital cavernous sinus. *Journal of Neurosurgery*, *86*(2), 252–262.

Carpenter, K., Decater, T., Iwanaga, J., Maulucci, C. M., Bui, C. J., Dumont, A. S., & Tubbs, R. S. (2021). Revisiting the vertebral venous plexus-a comprehensive review of the literature. *World Neurosurgery*, *145*, 381–395.

Chen, X. H., et al. (2004). MRI of the suboccipital cavernous sinus with thin sectional anatomy and computerized three-dimensional reconstruction. *Chinese Journal of Clinical Anatomy*, *22*(05), 469–472.

Chen, Y. J., et al. (2011). Three-dimensional CT anatomy of the vein behind atlantoaxial complex. *Journal of Clinical Rehabilitative Tissue Engineering Research*, *15*(52), 9787–9791.

Crockett, M. T., Chiu, A. H. Y., Singh, T. P., McAuliffe, W., & Phillips, T. J. (2019). Transvenous coil embolization with intra-operative cone beam CT assistance in the treatment of hypoglossal canal dural arteriovenous fistulae. *Journal of Neurointerventional Surgery*, *11*(2), 179–183.

Enix, D. E., Scali, F., & Pontell, M. E. (2014). The cervical myodural bridge, a review of literature and clinical implications. *The Journal of the Canadian Chiropractic Association*, *58*(2), 184–192.

Gao, H. B., et al. (2006). A new polyester technique for sheet plastination. *Journal of the International Society for Plastination*, *21*, 7–11.

George, T., & Tadi, P. (2022). Anatomy, head and neck, suboccipital muscles. In *StatPearls. Treasure Island*. StatPearls Publishing.

Geyik, A. M., Pusat, S., Alptekin, M., Ugur, B. K., Geyik, S., Nehir, A., & Erkutlu, I. (2021). Foramen magnum meningiomas: A report of 10 cases and literature review. *Turkish Neurosurgery*, *31*(6), 931–935.

Hack, G. D., & Hallgren, R. C. (2004). Chronic headache relief after section of suboccipital muscle dural connections: A case report. *Headache*, *44*(1), 84–89.

Hack, G. D., Koritzer, R. T., Robinson, W. L., Hallgren, R. C., & Greenman, P. E. (1995). Anatomic relation between the rectus capitis posterior minor muscle and the dura mater. *Spine (Phila Pa 1976)*, *20*(23), 2484–2486.

Haffajee, M. R., Thompson, C., & Govender, S. (2008). The supraodontoid space or "apical cave" at the craniocervical junction: A microdissection study. *Clinical Anatomy (New York, N.Y.)*, *21*(5), 405–415.

Hanakita, S., Oya, S., Tsuchiya, T., Shojima, M., & Matsui, T. (2019). Extirpation of a ruptured anterior spinal artery aneurysm accompanied by Dural arteriovenous fistula at the craniovertebral junction via a posterolateral approach: The Management of Extradural Venous Congestion. *Journal of Neurological Surgery, Part B, Skull Base*, *80*, S344–S345.

Hiramatsu, H., Sugiura, Y., Kamio, Y., & Kamiya, M. (2015). Transvenous embolization of a Dural arteriovenous fistula involving the suboccipital cavernous sinus. *Clinical Neuroradiology*, *25*(4), 419–422.

Holmes, D. F., et al. (2018). Collagen fibril assembly and function. *Current Topics in Developmental Biology*, *130*, 107–142.

Ibn Essayed, W., & Al-Mefty, O. (2021). Transcondylar odontoid resection and stabilization for craniovertebral degenerative compression: 2-dimensional operative video. *Oper Neurosurg (Hagerstown)*, *21*(5), E429–E430.

Iwanaga, J., Singh, V., Takeda, S., Ogeng'o, J., Kim, H.-J., Moryś, J., Ravi, K. S., Ribatti, D., Trainor, P. A., Sañudo, J. R., Apaydin, N., Sharma, A., Smith, H. F., Walocha, J. A., Hegazy, A. M. S., Duparc, F., Paulsen, F., del Sol, M., Adds, P., … Tubbs, R. S. (2022). Standardized statement for the ethical use of human cadaveric tissues in anatomy research papers: Recommendations from anatomical journal editors-in-chief. *Clinical Anatomy (New York, N.Y.)*, *35*(4), 526–528.

Jagetia, A., Dutta, G., Setia, V., Singhal, G. D., Bodeliwala, S., & Srivastava, A. K. (2019). Dissection of C2 guiding to C1 lateral mass and facilitation of screw placement: Technical note. *World Neurosurgery*, *126*, 237–240.

JIANG, S. M., et al. (2022). A comparative study of the morphology of suboccipital cavernous sinus using magnetic resonance imaging and cast specimens. *International Journal of Morphology*, *40*(4), 1000–1008.

Joe, I., et al. (2021). Acknowledging the use of human cadaveric tissues in research papers: Recommendations from anatomical journal editors. *Clinical Anatomy (New York, N.Y.)*, *34*(1), 2–4.

Kitamura, K., et al. (2019). Suboccipital myodural bridges revisited: Application to cervicogenic headaches. *Clinical Anatomy (New York, N.Y.)*, *32*(7), 914–928.

Kontautas, E., Ambrozaitis, K. V., Spakauskas, B., & Smailys, A. (2005). Upper cervical spine injuries and their diagnostic features. *Medicina (Kaunas, Lithuania)*, *41*(9), 802–809.

Ma, Y., et al. (2021). The morphology, biomechanics, and physiological function of the suboccipital myodural connections. *Scientific Reports*, 2021, *11*(1), 8064.

Nathoo, N., Caris, E. C., Wiener, J. A., & Mendel, E. (2011). History of the vertebral venous plexus and the significant contributions of Breschet and Batson. *Neurosurgery*, *69*(5), 1007–1014.

Nowaczewska, M., & Kaźmierczak, H. (2019). Cerebral blood flow in low intracranial pressure headaches-what is known? *Brain Sciences*, *10*(1), 2.

Park, J. S., et al. (2009). Sectioned images of the cadaver head including the brain and correspondences with ultrahigh feld 7.0 T MRIs. *Proceedings of the IEEE*, *97*(12), 1988–1996.

Pontell, M. E., et al. (2013). The obliquus capitis inferior myodural bridge. *Clinical Anatomy (New York, N.Y.)*, *26*, 450–454, 4.

Scali, F., et al. (2013). Histological analysis of the rectus capitis posterior major's myodural bridge. *The Spine Journal: Official Journal of the North American Spine Society*, *13*(5), 558–563.

Sui, H. J., & Henry, R. W. (2007). Polyester plastination of biological tissue: Hoffen P45 technique. *Journal of the International Society for Plastination*, *22*, 78–81.

Takahashi, S., Sakuma, I., Omachi, K., Otani, T., Tomura, N., Watarai, J., & Mizoi, K. (2005). Craniocervical junction venous anatomy around the suboccipital cavernous sinus: Evaluation by MR imaging. *European Radiology*, *15*(8), 1694–1700.

Tanoue, S., Kiyosue, H., Sagara, Y., Hori, Y., Okahara, M., Kashiwagi, J., & Mori, H. (2010). Venous structures at the craniocervical junction: Anatomical variations evaluated by multidetector row CT. *The British Journal of Radiology*, *83*(994), 831–840.

Testa, S., Costantini, M., Fornetti, E., Bernardini, S., Trombetta, M., Seliktar, D., Cannata, S., Rainer, A., & Gargioli, C. (2017). Combination of biochemical and mechanical cues for tendon tissue engineering. *Journal of Cellular and Molecular Medicine*, *21*(11), 2711–2719.

Venne, G., Rasquinha, B. J., Kunz, M., & Ellis, R. E. (2017). Rectus capitis posterior minor: Histological and biomechanical links to the spinal dura mater. *Spine*, *42*(8), E466–E473.

Wang, Z., Wang, X., Wu, H., Chen, Z., Yuan, Q., & Jian, F. (2016). C2 dumbbell-shaped peripheral nerve sheath tumors: Surgical management and relationship with venous structures. *Clinical Neurology and Neurosurgery*, *151*, 96–101.

Xu, Q., Yu, S. B., Zheng, N., Yuan, X. Y., Chi, Y. Y., Liu, C., Wang, X. M., Lin, X. T., & Sui, H. J. (2016). Head movement, an important contributor to human cerebrospinal fluid circulation. *Scientific Reports*, *6*, 31787.

Young, B. A., et al. (2020). The myodural bridge of the American alligator (Alligator mississippiensis) alters CSF flow. *The Journal of Experimental Biology*, *223*(Pt 22), jeb230896.

Yuan, X. Y., Yu, S. B., Li, Y. F., Chi, Y. Y., Zheng, N., Gao, H. B., Luan, B. Y., Zhang, Z. X., & Sui, H. J. (2016). Patterns of attachment of the myodural bridge by the rectus capitis posterior minor muscle. *Anatomical Science International*, *91*(2), 175–179.

Yuan, X. Y., Yu, S. B., Liu, C., Xu, Q., Zheng, N., Zhang, J. F., Chi, Y. Y., Wang, X. G., Lin, X. T., & Sui, H. J. (2017). Correlation between chronic headaches and the rectus capitis posterior minor muscle: A comparative analysis of cross-sectional trail. *Cephalalgia: An International Journal of Headache*, *37*(11), 1051–1056.

Zheng, N., Chi, Y. Y., Yang, X. H., Wang, N. X., Li, Y. L., Ge, Y. Y., Zhang, L. X., Liu, T. Y., Yuan, X. Y., Yu, S. B., & Sui, H. J. (2018). Orientation and property of fibers of the myodural bridge in humans. *The Spine Journal: Official Journal of the North American Spine Society*, *18*(6), 1081–1087.

Zheng, N., Chung, B. S., Li, Y. L., Liu, T. Y., Zhang, L. X., Ge, Y. Y., Wang, N. X., Zhang, Z. H., Cai, L., Chi, Y. Y., Zhang, J. F., Samuel, O. C., Yu, S. B., & Sui, H. J. (2020). The myodural bridge complex defined as a new functional structure. *Surgical and Radiologic Anatomy*, *42*(2), 143–153.

Zheng, N., Yuan, X. Y., Li, Y. F., Chi, Y. Y., Gao, H. B., Zhao, X., Yu, S. B., Sui, H. J., & Sharkey, J. (2014). Definition of the to be named ligament and vertebrodural ligament and their possible effects on the circulation of CSF. *PLoS One*, *9*(8), e103451.

How to cite this article: Zhang, X.-H., Gong, J., Song, Y., Hack, G. D., Jiang, S.-M., Yu, S.-B., Song, X., Zhang, J., Yang, H., Cheng, J., Sui, H.-J., & Zheng, N. (2023). An anatomical study of the suboccipital cavernous sinus and its relationship with the myodural bridge complex. *Clinical Anatomy*, *36*(5), 726–736. https://doi.org/10.1002/ca.24048